



A simple ImageJ macro tool for analyzing mitochondrial network morphology in mammalian cell culture



Andrew J. Valente^a, Lucas A. Maddalena^a, Ellen L. Robb^b, Fereshteh Moradi^a, Jeffrey A. Stuart^{a,*}

^a Department of Biology, Brock University, St. Catharines, Ontario, Canada, L2S 3A1

^b Michael G. DeGroote School of Medicine, McMaster University, Hamilton, Ontario, Canada L8S 4L8

ARTICLE INFO

Article history:

Received 2 December 2016

Received in revised form 7 February 2017

Accepted 3 March 2017

Keywords:

Mitochondria

Fusion

Fission

Mitochondrial network

Image analysis

Mitochondrial dynamics

ABSTRACT

Mitochondria exist in a dynamic cycle of fusion and fission whose balance directly influences the morphology of the 'mitochondrial network', a term that encompasses the branched, reticular structure of fused mitochondria as well as the separate, punctate individual organelles within a eukaryotic cell. Over the past decade, the significance of the mitochondrial network has been increasingly appreciated, motivating the development of various approaches to analyze it. Here, we describe the Mitochondrial Network Analysis (MiNA) toolset, a relatively simple pair of macros making use of existing ImageJ plug-ins, allowing for semi-automated analysis of mitochondrial networks in cultured mammalian cells. MiNA is freely available at <https://github.com/StuartLub>. The tool incorporates optional preprocessing steps to enhance the quality of images before converting the images to binary and producing a morphological skeleton for calculating nine parameters to quantitatively capture the morphology of the mitochondrial network. The efficacy of the macro toolset is demonstrated using a sample set of images from SH-SY5Y, C2C12, and mouse embryo fibroblast (MEF) cell cultures treated under different conditions and exhibiting hyperfused, fused, and fragmented mitochondrial network morphologies.

© 2017 Elsevier GmbH. All rights reserved.

1. Introduction

In live cells, mitochondria undergo fusion and fission to continuously re-model a dynamic, interconnected mitochondrial network that affects cellular functions beyond ATP homeostasis. Normal mitochondrial fusion and fission is essential for mtDNA maintenance (Chen et al., 2010), cell cycle progression, and metabolic regulation (reviewed in Lee and Finkel, 2013; Salazar-Roa and Malumbres, 2016). Dysregulation of mitochondrial dynamics underlies some heritable diseases, including Charcot-Marie-Tooth Type IIA (Tufano et al., 2015). The importance of mitochondrial dynamics to normal and aberrant cell function has motivated the development of tools for its analysis.

Fluorescence confocal microscopy of live or fixed cells has been the primary approach taken for capturing 'snapshots' of the mitochondrial network. Initial approaches to evaluating the resultant images included qualitatively 'binning' mitochondrial structures into categories of 'fused', 'fragmented', and 'intermediate' mor-

phologies (Mitra et al., 2009). More recently, software-based approaches allowing more quantitative and objective analyses have been developed (Ahmad et al., 2013; Koopman et al., 2006; Leonard et al., 2015; Lihavainen et al., 2012; Niklaisen et al., 2014). The approaches take on a variety of forms, incorporating machine-learning practices (Ahmad et al., 2013; Koopman et al., 2006; Leonard et al., 2015) and more direct approaches to measuring the mitochondrial features (Lihavainen et al., 2012; Niklaisen et al., 2014). One drawback of these methods for mitochondrial network analysis is that their implementation relies on commercial software such as Matlab, ImagePlus Pro, and GE INCell. Open source alternatives do exist, such as MitoMap and Mito-Morphology, which run in ImageJ (Dagda, 2010; Vowinkel et al., 2015). MitoMap (<http://www.gurdon.cam.ac.uk/institute-life/downloadspublic/imaging-plugins>) is suitable for extracting physical information about mitochondrial structures, but only from high resolution three dimensional datasets which are not always available. Mito-Morphology (http://imagejdocu.tudor.lu/doku.php?id=plugin:morphology:mitochondrial_morphology_macro_plugin:start) is strictly for two dimensional analysis. The Mito-Morphology set of macros uses a host of parameters determined from the area, perimeter, and elliptical fitting of

* Corresponding authors.

E-mail addresses: jstuart@brocku.ca (J.A. Stuart).

fluorescently labelled features to capture the morphology of the mitochondrial material within a cell. However, it does not measure branching of mitochondrial networks, and is more useful for cells exhibiting larger, rounder mitochondria as several of the measurements are based on elliptical approximation.

Cultured, adherent mammalian cells often exhibit tubular connected mitochondrial morphologies and cannot always be imaged in three dimensions using super-resolution capable devices. This motivated our development of the Mitochondrial Network Analysis tool (MiNA), which uses the freely available FIJI distribution of the ImageJ platform and amalgamates open source tools into a simple macro toolset with a user-friendly interface (for more on FIJI and ImageJ, see Schindelin et al., 2012; Schneider et al., 2012). The code is readily accessible and can therefore be modified to suit the needs of the user. The macro is largely inspired by Nikolaisen et al. (2014). The goal of MiNA is to provide simplified image analysis methods to biologists on a familiar platform that is expandable and free. MiNA was developed to evaluate the extent of mitochondrial branching and therefore to distinguish between unbranched structures, like unbranched puncta and rods (individuals), and branched structures (networks). In addition to identifying networks, MiNA will evaluate the extent of branching within individual networks, thus identifying cells in which mitochondria are ‘hyper-fused’, i.e. have very highly branched mitochondrial networks. Since both highly fragmented mitochondria (associated with specific cell cycle phases, depolarization, mitophagy) and highly fused mitochondria (associated with specific cell cycle phases, states of high aerobic metabolic activity) have important implications in cell biology (Babbar and Sheikh, 2013; Galloway et al., 2012; Mitra et al., 2009; Rossignol et al., 2004), the ability to accurately identify these states is critical. Here we present and validate MiNA as a free open source tool for analyzing the extent of mitochondrial network fusion in cultured, adherent mammalian cells.

2. Materials and methods

2.1. Materials

C2C12 cells, Dulbecco's Modified Eagle Medium (DMEM), Modified Eagle Medium (MEM) containing non-essential amino acids, and fetal bovine serum were purchased from Sigma-Aldrich (St. Louis, MO, USA). SH-SY5Y cells were obtained from ATCC (Manassas, VA, USA). Wild-type (wt) mouse embryonic fibroblasts (MEFs) and Mfn2-null MEFs were obtained from Jackson Laboratory (Bar Harbor, Maine, USA). MitoTracker Red CMXRos was purchased from Life Technologies (Burlington, ON, Canada). The mEmerald-Mito-7 plasmid encoding a mitochondria-targeted modified emerald fluorescent protein was a generous gift from Michael Davidson (Addgene plasmid #54160; Planchon et al., 2011). All other reagents were obtained from either Sigma-Aldrich or BioShop (Burlington, ON, Canada).

2.2. Cell culture

C2C12 cells, SH-SY5Y cells, wtMEFs, and Mfn2-null MEFs were maintained as instructed by distributor protocols and cultured in DMEM containing 4500 mg/L glucose, 4 mM L-glutamine and 1 mM sodium pyruvate and further supplemented with 10% fetal bovine serum, 2X MEM containing non-essential amino acids, and penicillin (50 I.U./mL)/streptomycin (50 µg/mL) solution. All cell lines were grown within an incubator containing a humidified, 37 °C, atmospheric O₂/5% CO₂ environment, unless otherwise indicated. For resveratrol (10 µM, 48 h) and carbonylcyanide-p-trifluoromethoxyphenylhydrazone (FCCP; 1 µM, 3 h) treatments, media on dishes was replaced with pre-warmed culture media

containing the freshly added chemical. For experiments involving hypoxia exposure, cells were placed within a humidified hypoxic chamber that was purged with 95% N₂/5% CO₂ gas mix until O₂ levels reached 0.1%. The chamber was sealed and kept within a humidified, 37 °C, 3% O₂/5% CO₂ incubator for 24 h.

2.3. Fluorescence labelling of mitochondria

An SH-SY5Y cell line stably expressing a mitochondria-targeted modified emerald fluorescent protein (mito-mEFP) was generated as in Maddalena et al. (2017). Alternatively, mitochondria in C2C12 cells and MEFs were labelled with MitoTracker Red CMXRos. This was achieved by incubating the cells with culture media containing 20 nM dye for 30 min within the culture incubator, followed by washing several times with pre-warmed phosphate-buffered saline.

2.4. Live-cell fluorescence microscopy

Fluorescence images of live cells were obtained using a Carl Zeiss Axio Observer.Z1 inverted light/epifluorescence microscope equipped with ApoTome.2 optical sectioning, a Plan-Apochromat 63x/1.40 oil objective, and a Hamamatsu ORCA-Flash4.0 V2 digital camera. Green fluorescence from mEFP was measured using a 450–490 nm excitation and 500–550 nm emission filter set. Red fluorescence from MitoTracker Red CMXRos was detected using a 540–552 nm excitation and 590–660 nm emission filter set. Excitation (set at 488 nm and 587 nm, respectively) was achieved with an X-Cite 120LED light source. Z-stack series consisted of 0.25 to 0.3 µm slice intervals and were rendered into single 2D images using the “extended depth of focus” processing tool using Zeiss Zen 2 software. All live cells were imaged on MatTek (Ashland, MA, USA) 35 mm poly-D-lysine-coated glass bottom culture dishes containing phenol red-free culture media. The microscope stage was maintained at 37 °C with humidified 5% CO₂ air during imaging. For imaging of cells exposed to 24 h hypoxia, the stage was maintained at 37 °C with in-flow of humidified 95% N₂/5% CO₂ gas mix.

2.5. Analysis of mitochondrial morphology

The analysis method utilizes two ImageJ Macro Tools, one for batch analysis and another for processing a single image or region of interest (ROI). These tools, and documentation regarding their usage, are available at <https://github.com/StuartLub>. The FIJI distribution of ImageJ on which the macros are designed to run is available at <https://fiji.sc/>. An overview of the workflow for pre-processing and analysis of images is presented in Fig. 1.

2.6. Image pre-processing using MiNA

Accurate analysis of mitochondrial network morphology requires sharp, high contrast images exhibiting minimal noise. In practice, images obtained from confocal fluorescence microscopy are often blurred due to the diffraction effects of the system, especially when considering that the size of mitochondria requires the microscope to be resolving features near its diffraction limit (~1/2 the excitation wavelength in a confocal system). MiNA provides includes options to enhance the image quality prior to analysis to provide more accurate results. Choices for image pre-processing, including ‘unsharp mask’, CLAHE, and median filtering are presented to the user through the MiNA interface.

Unsharp masking, included in the ImageJ package (Ferreira and Rasband, 2012), provides a fast method for enhancing the sharpness of an image by subtracting a blurred copy of the image from the original and rescaling the histogram to produce the original contrast in low frequency features (Fig. 2A and B) (“Class

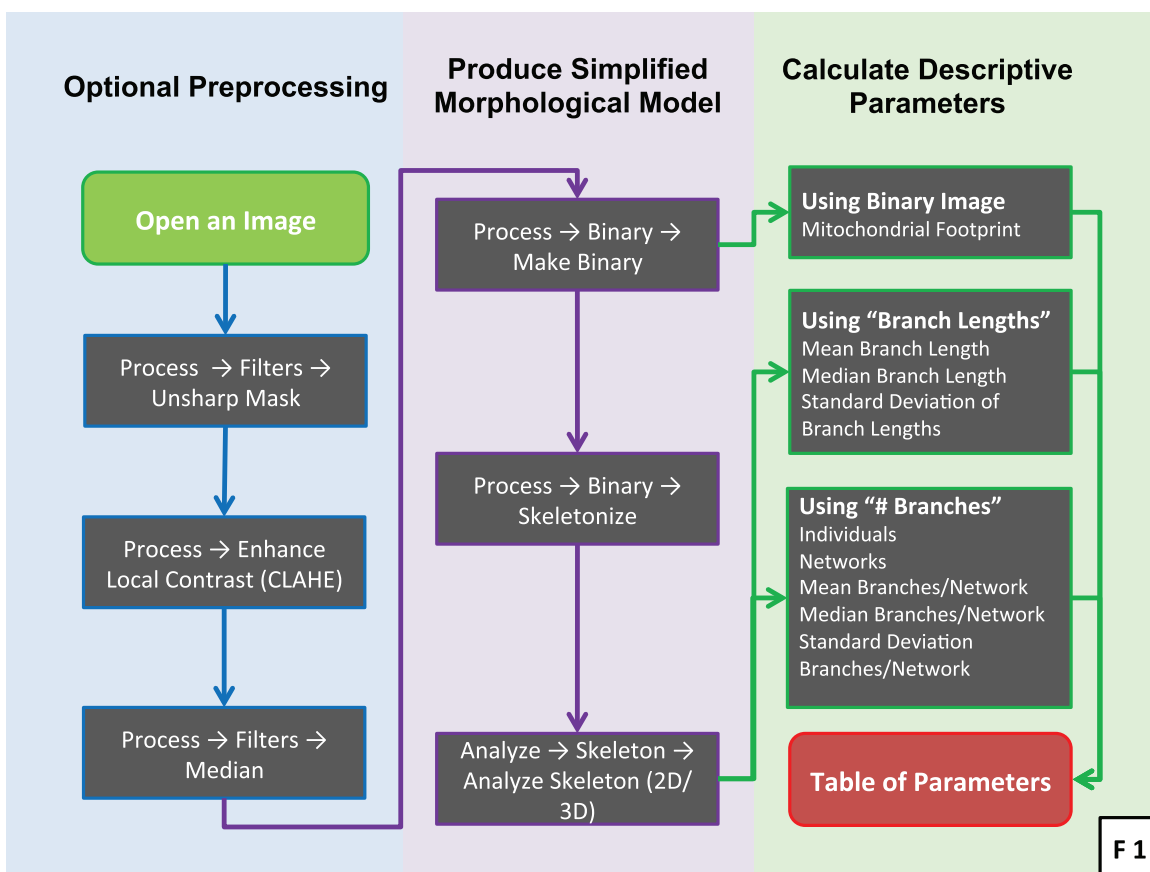


Fig. 1. MiNA workflow. Images are pre-processed to improve quality prior to binarizing and skeletonizing. Note that the pre-processing steps are sequential but each is optional. It is the user's choice to omit any or all steps. Mitochondrial footprint, i.e. the area occupied by mitochondrial structures is calculated from the binarized image prior to skeletonizing. Descriptive parameters are calculated from the skeletonized image.

"UnsharpMask," n.d.). MiNA uses this process in place of deconvolution or top hat filtering, which has been employed by others (Koopman et al., 2006; Leonard et al., 2015; Lihavainen et al., 2012; Nikolaisen et al., 2014), as it produces a similar visual result without the need for additional plugins. However, the top hat filter used by Koopman and described in detail by Iannetti et al. (2016) is included in the MiNA toolset as an alternative means of pre-processing images.

Contrast limited adaptive histogram equalization (CLAHE) adjusts the pixel intensities to equalize the histogram throughout the image using a given block size, but limiting how much local change is allowed to inhibit over-amplification of noise (Fig. 2C) (Saalfeld, 2010). This can be useful when images, or certain regions within an image, appear dim. The CLAHE process is available to ImageJ via a plugin or included in the FIJI distribution (Saalfeld, 2010). Contrast enhancement using CLAHE can be applied using different block sizes, histogram bins, and maximal slopes. The MiNA macros use a 127 pixel block size, 256 histogram bins, and a maximum slope of 3 by default.

Fluorescent images often contain salt and pepper noise, which can be greatly amplified by unsharp masking and CLAHE. Median filtering provides a convenient way to reduce or eliminate this type of noise (Fig. 2D). This method preserves edges better than mean filtering which blurs edges as it averages real signal with the background. The filter is applied to a specified radius of two pixels. Using this, the pixel value is changed to the median of the surrounding pixels within a two pixel radius, removing noise. Median filtering functionality is included in both the ImageJ and FIJI packages (Ferreira and Rasband, 2012).

2.7. Image analysis

For analysis, the image is first converted to binary (Fig. 2E) by thresholding, where a foreground pixel is assigned the maximum value (255) and background pixels are assigned the minimum possible value (0). This is done using ImageJ's default thresholding method, referred to as IsoData (Landini, 2016) and adapted from Ridler and Calvard (1978). This method incrementally selects a threshold value until $\text{Threshold Value} > (\bar{I}_{\text{Below}} + \bar{I}_{\text{Above}})/2$, where \bar{I}_{Below} is the average pixel intensity of pixels below the threshold and \bar{I}_{Above} is the average pixel intensity of pixels above the threshold value (Landini, 2016).

Using the ImageJ built in 'Skeletonize' feature, the binary image is then converted to a skeleton that represents the features in the original image using a wireframe of lines one pixel wide (Fig. 2F) (Ferreira and Rasband, 2012). This process employs the algorithm presented by Zhang and Suen, which uses parallel sub-iterations to thin features by removing external pixels (Ferreira and Rasband, 2012; Guo and Hall, 1989).

All pixels within a skeleton are then grouped into three categories: end point pixels, slab pixels, and junction pixels (Fig. 3) using Ignacio Arganda-Carreras' 'AnalyzeSkeleton' plugin. The plugin was originally written for analyzing mammary gland tissue (Arganda-Carreras et al., 2010). This plugin classifies each pixel of a skeleton, then uses how the pixels are spatially related and defined to measure the length of each branch and the number of branches in each skeletonized feature (Arganda-Carreras, 2016). To simplify the analysis, the MiNA macro strips the branch length and the number of branches in each skeletonized feature from the AnalyzeSkeleton

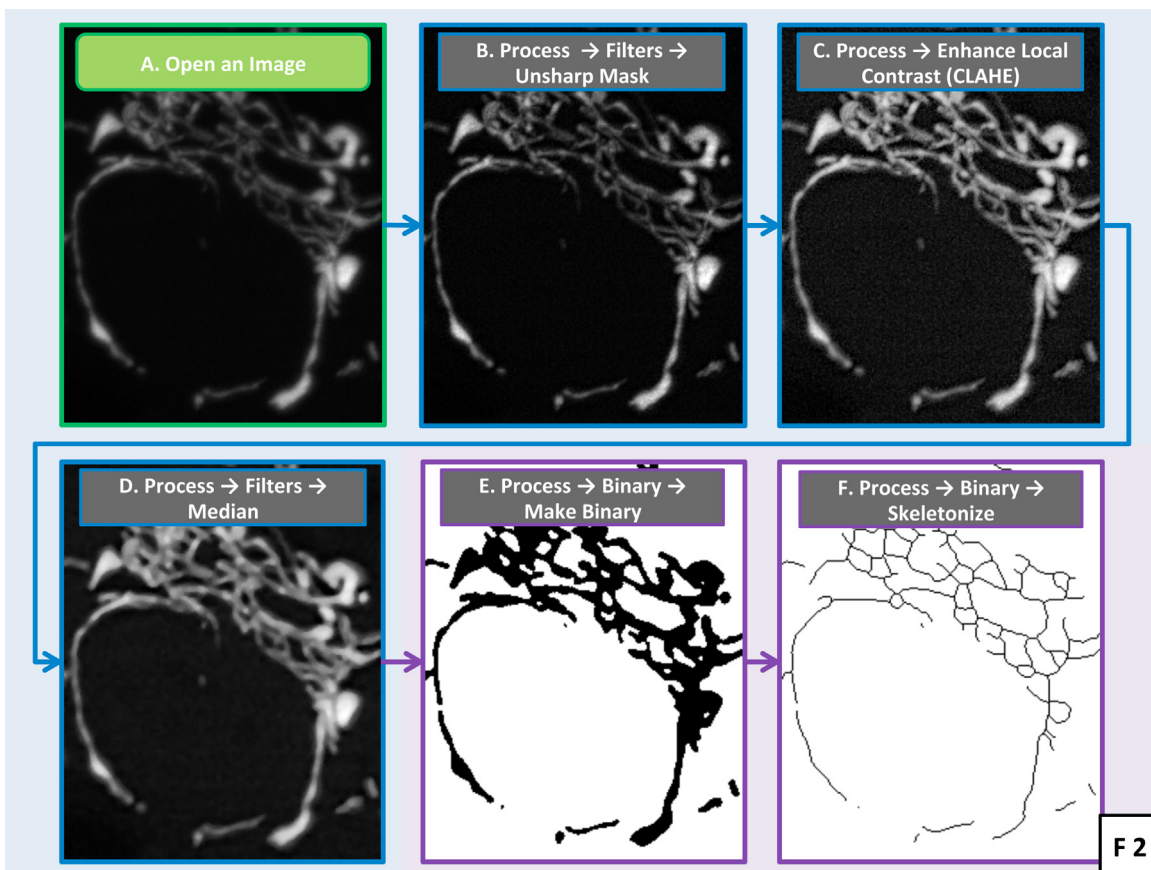


Fig. 2. Preparation of an image of a single SH-SY5Y cell expressing mito-mEFP to prepare for mitochondrial network feature analysis. (A) The original image is processed using (B) unsharp mask, (C) CLAHE, and (D) median. The image is then (E) binarized and (F) skeletonized.

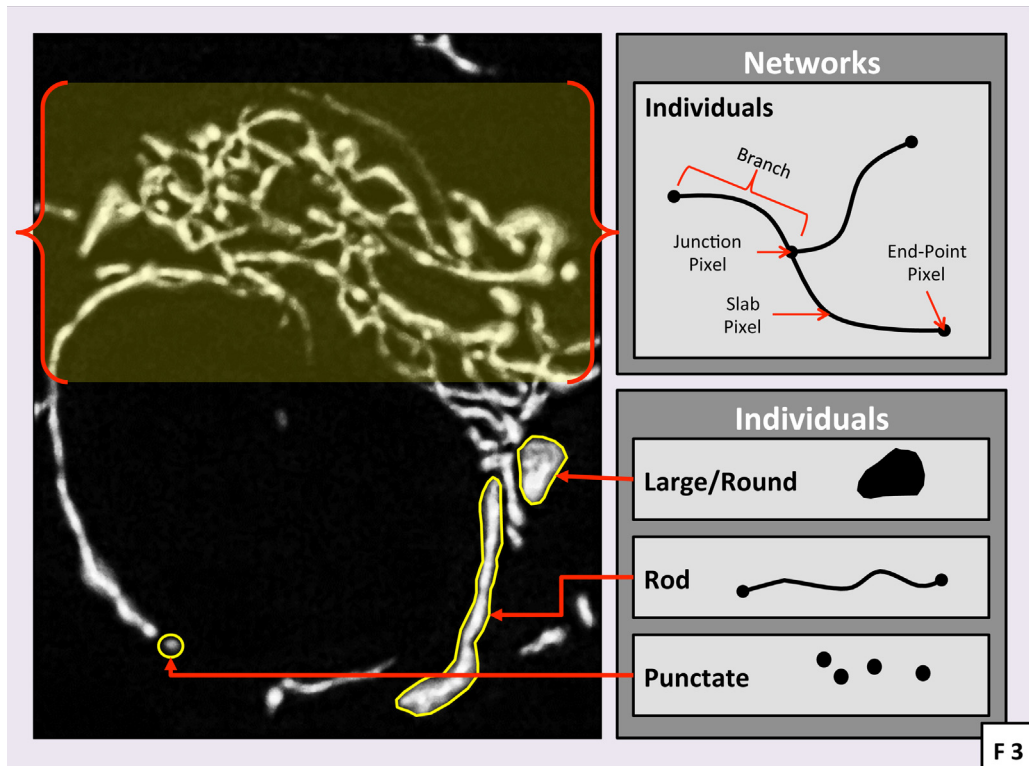


Fig. 3. Examples of common mitochondrial network features. MiNA will recognize only two types of mitochondrial structures in a skeletonized image: networks and individuals. Individuals are punctate (a single pixel in the skeletonized image), rods (unbranched structures with two or more pixels in the skeletonized image), and large/round structures (which are reduced to rods, or occasionally small networks, during skeletonization). Networks are mitochondrial structures with at least a single node and three branches.

plugin's output and places them into arrays, from which parameters describing mitochondrial network morphology are calculated.

Individual investigators have defined the morphologies of mitochondrial structures differently and using a wide variety of terms including tubular, donut, blob, 'small sausage-like', 'long snake-like', branched reticula, extended filaments and networks, and clustered (Ahmad et al., 2013; Koopman et al., 2006). The nomenclature used by MiNA was adopted and modified from Leonard et al. (2015). Leonard recognized four distinct morphologies: puncta, rods, networks, and 'large and round' structures. Punctate mitochondria are defined as small point like structures, whereas rods are elongated without being branched. Networks are characterized by connected branches, which can be extensive in some instances. Large and round mitochondrial structures are essentially very large puncta – round structures occupying significant volume (Leonard et al., 2015). MiNA recognizes only two distinct object types: 'individuals' (no junctions) and 'networks' (structures with at least one junction) (Fig. 3). For these two object types, MiNA computes nine parameters: number of 'individual' structures with no

branches (puncta and rods), number of networks, mean length of rods/network branches, median length of rods/network branches, standard deviation of rod/network branch lengths, mean number of branches per network, median number of branches per network, standard deviation of the number of branches per network, and the mitochondrial footprint (this is calculated prior to skeletonization) (Table 1). It is important to note that the calculated length parameters (e.g. mean length of rods/network branches) consider rods (which are not connected to a network) and network branches together (puncta lengths are not included in the analysis). This is because we presume that the biological forces increasing rod length are essentially the same as those increasing the lengths of network branches.

2.8. Evaluating MiNA output

Seven of the nine parameters in the output tables were compared between groups using boxplots generated using the statistics programming language R (R Core Team, 2016) and the plotting

Table 1

Parameter ^a	Description	Parameter expression or explanation ^b
filepath ^c	This is the complete filepath for the image processed by the Batch Analysis macro.	Accessed using getFileList in the Batch Macro.
Individuals <i>individuals</i>	This is the number of objects in the image that do not contain a junction pixel and thus are comprised of 1 or 0 branches (0 branches being a point). Also referred to as punctate and rods.	$\sum_{n=0}^{n=N} B_n \leq 1$
Networks <i>networks</i>	This is the number of objects in the image that contain at least 1 junction pixel and are thus comprised of more than one branch.	$\sum_{n=0}^{n=N} B_n > 1$
Mean Length of Rods/Branches <i>meanLength</i>	The average length of all rods/branches.	$\frac{1}{N} \sum_{n=0}^{n=N} L_n$
Median Length of Rods/Branches <i>medianLength</i>	The median rod/branch length is the middlemost value of all rod/branch lengths when sorted or the mean of the two most medial values if there is an even number of rods/branches.	If odd array size: $Sort(L)_{((N-1)/2)}$ If even array size: $(Sort(L)_{N/2} + Sort(L)_{(N/2)-1})/2$
Length Standard Deviation <i>lengthStandardDeviation</i>	This is the standard deviation of all rod/branch lengths treated as a population.	$\sqrt{\frac{\sum_{n=0}^{n=N} (L_n - \bar{L})^2}{N}}$
Mean Network Size (Branches) <i>meanNetworkSize</i>	This is the mean number of branches per network.	$\frac{1}{N} \sum_n b_n$
Median Network Size (Branches) <i>medianNetworkSize</i>	The median network size is the middlemost value of all branch counts per network when sorted or the mean of the two most medial values if there is an even number of networks.	If odd array size: $Sort(b)_{((N-1)/2)}$ If even array size: $(Sort(b)_{N/2} + Sort(b)_{(N/2)-1})/2$
Network Size Standard Deviation <i>networkSizeStandardDeviation</i>	This is the standard deviation of the number of branches per network as a population.	$\sqrt{\frac{\sum_{n=0}^{n=N} (B_n - \bar{B})^2}{N}}$
Mitochondrial Footprint <i>mitochondrialFootprint</i>	This is the total area in the image consumed by signal after being separated from the background. It is the number of pixels in the binary image containing signal multiplied by the area of a pixel if the calibration information is present.	Let I represent the pixel intensity in the binarized image, s represent the calibrated length of one pixel, x represent the width of the image in pixels, and y represent the height of the image in pixels. $\frac{\text{average}}{\text{maximum}} \times x \times y \times s^2$

^a Variable names as shown in the Single Image macro are shown in standard font first, while the equivalent in the output table of the Batch Analysis macro are shown in italics underneath. The variation in naming convention is to remove spaces so the variable names may be used as headers for that macro.

^b The variable L represents the array of branch lengths, B represents the array of branches per network, and b is the subset of B such that $B_i > 1$. Note that logical operators, such as = (equal to), < (less than), and > (greater than), return 1 for true and 0 for false in the ImageJ macro language. Also, indexing is given from $n = 0$ to $n = N$, where N is the length of the array minus 1 as indexing begins at 0.

^c filepath is only a variable in the Batch Analysis macro.

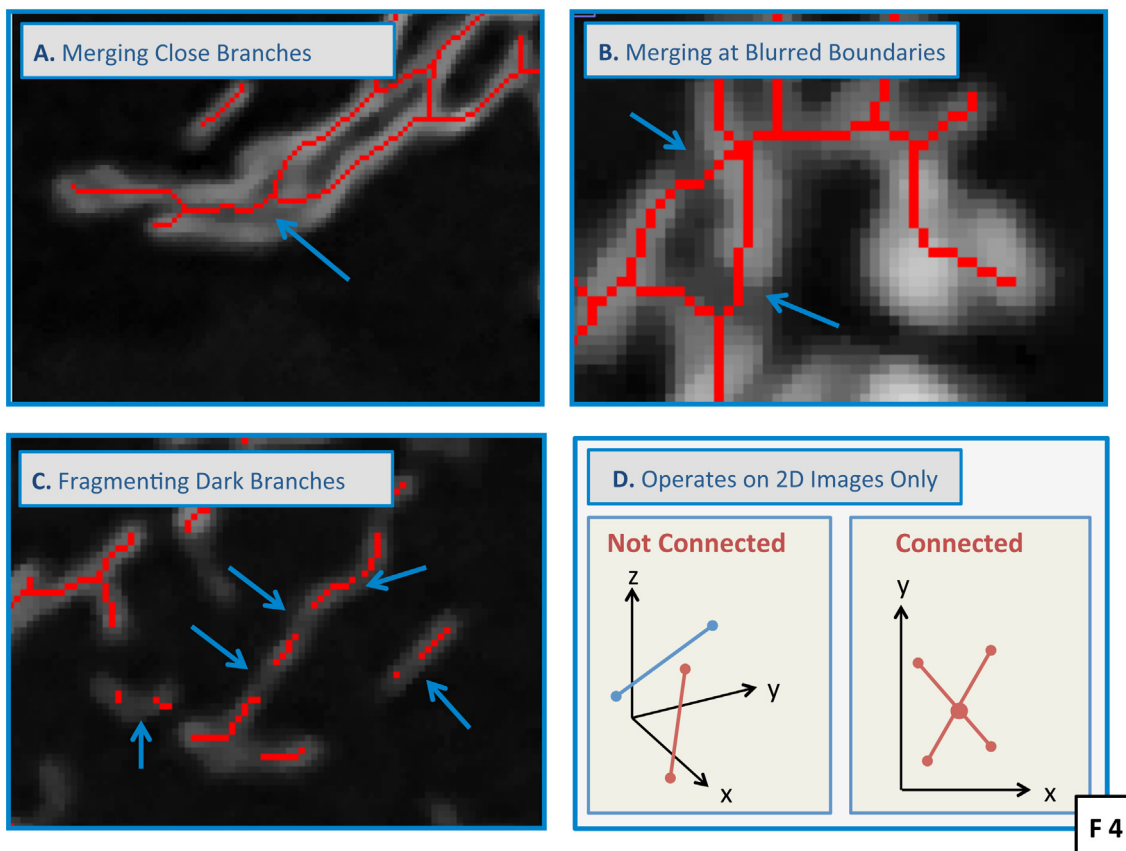


Fig. 4. Common issues that compromise the ability of MiNA to generate an accurate skeleton. (A) Positionally close branches may be merged. (B) Blurring at boundaries exacerbates issue (A). (C) Inhomogeneous contrast can lead to erroneous fragmentation of images. (D) The analysis is constrained to work on 2-dimensional images. The accuracy of the skeleton will therefore be reduced in thicker cells.

library ggplot2 (Wickham, 2009). The results were compared using Kruskal–Wallis statistical tests included in the R base library and the multiple comparison kruskalmc functionality of the pgrirmess library (Giraudoux, 2016) for MEF cells.

3. Results and discussion

Images obtained from cultured SH-SY5Y, MEFs, and C2C12 cell lines were processed using the MiNA Single Image macro and the MiNA Batch Analysis macro to investigate the efficacy of the pre-processing and accuracy of the subsequent analysis on different cell types under different treatment conditions. A variety of treatment conditions and genotypes (mitofusin-2 null cells) known to be associated with enhanced network hyper-fusion or fragmentation were chosen to allow evaluation of how well MiNA could detect and quantify these different morphological features.

The goal of MiNA is to estimate the mitochondrial network skeleton in representative images of a single cell and then compute values describing that skeleton. The accuracy of the skeleton is affected by several artifacts (Fig. 4) which must be eliminated or at least minimized for the analysis to be accurate. There are three main artifacts associated with image quality. Mitochondrial structures close in proximity to each other may be erroneously merged into a single structure (Fig. 4A). This artifactual merging is exacerbated when the images of mitochondrial structures are blurred due to optical diffraction and out of focus light (Fig. 4B). On the other hand, where there is inhomogeneous contrast between foreground and background within an image, single structures can be erroneously fragmented into multiple structures (Fig. 4C). In addition to these artifacts, which must be evaluated and corrected, a

separate limitation of MiNA arises from the fact that it analyzes 2-dimensional images taken of 3-dimensional cells. Mitochondrial structures at different positions on the z-axis can be erroneously categorized as branched (Fig. 4D). To minimize the contribution of this artifact to computed network parameter values, MiNA should be restricted to use with adherent mammalian cells growing as relatively flat monolayers with minimal thickness.

Using images from fourteen SH-SY5Y cells expressing a mito-mEFP (Maddalena et al., 2017), the efficiencies of MiNA's preprocessing steps (which occur sequentially) were evaluated (Fig. 5A). The process is shown in detail for a single representative image, which was pre-processed using unsharp mask, CLAHE, and median filtering. It was then skeletonized and analyzed (Fig. 5A). This process was repeated in the SH-SY5Y cells that had been treated with 1 μ M FCCP for 3 h (Fig. 5B). FCCP is a protonophore that uncouples mitochondrial oxidative phosphorylation and causes extensive network fragmentation (Benard et al., 2007; Cereghetti et al., 2010; Ishihara et al., 2006; Legros et al., 2002; Liu and Hajnóczky, 2011). The network parameter values were then calculated (Fig. 5C). FCCP increased the number of individuals (puncta and rods). It also increased the number of networks. However, this latter observation was related to the fragmentation of larger networks with more branches into many smaller networks, as seen in the decrease in number of branches per network. Mitochondrial footprint (calculated before pre-processing) was also reduced by FCCP treatment, perhaps relating to mitophagy of the fragmented mitochondria (Twig et al., 2008). Overall, MiNA effectively captured the visually apparent fragmentation of larger mitochondrial networks into smaller structures upon FCCP treatment.

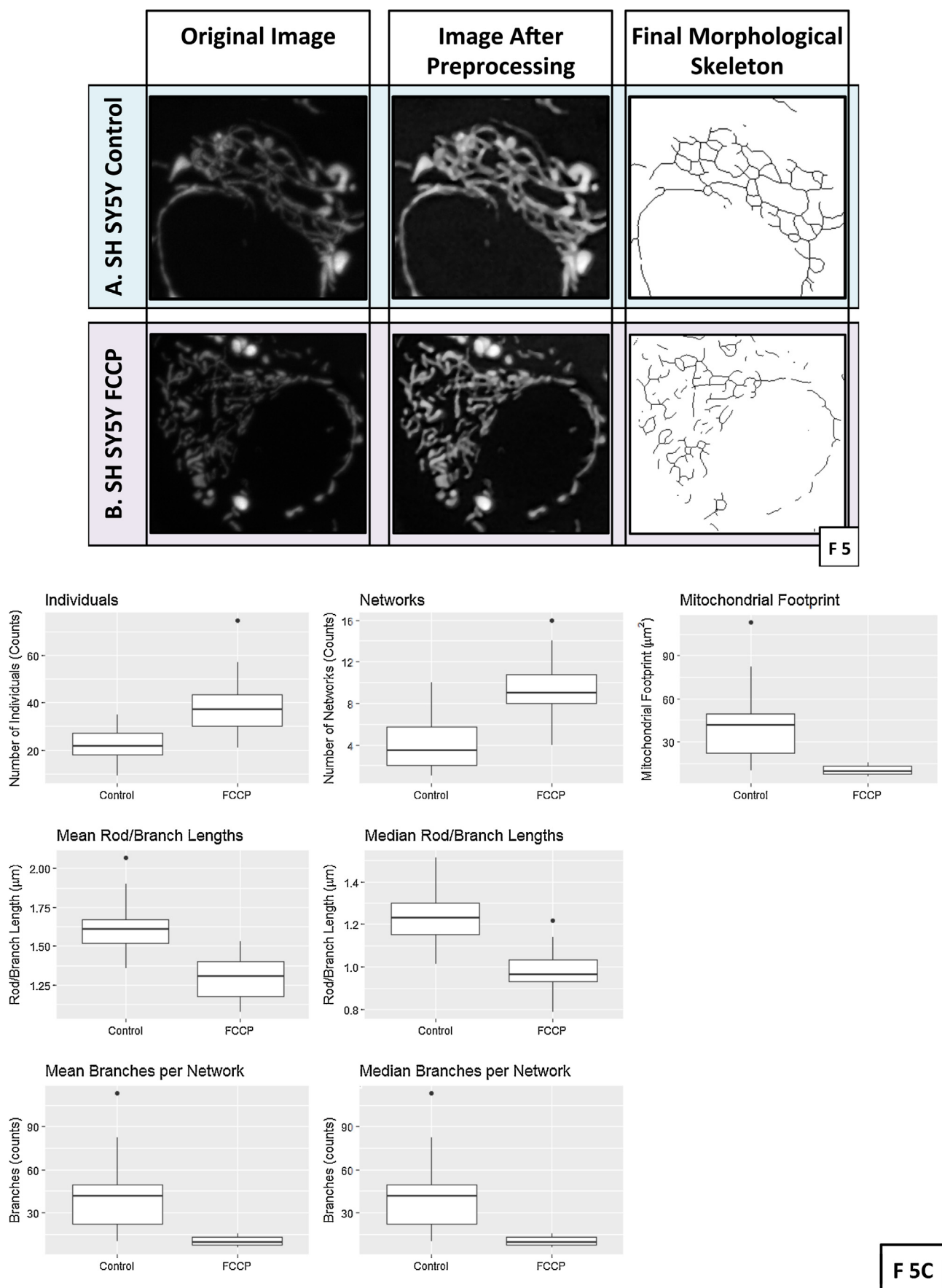


Fig. 5. Results from mitochondrial network analysis performed on fourteen SH-SY5Y cells. (A) A single control cell untreated. (B) A single cell treated with 1 μM FCCP for 3 h. (C) Summary statistics for all cells. Box plots show median (horizontal lines), first to third quartile (box), and the most extreme values within 1.5 times the interquartile range (vertical lines). For all comparisons, differences between control and FCCP treated cells were statistically significant ($p < 0.05$), using Kruskal Wallis test in R.

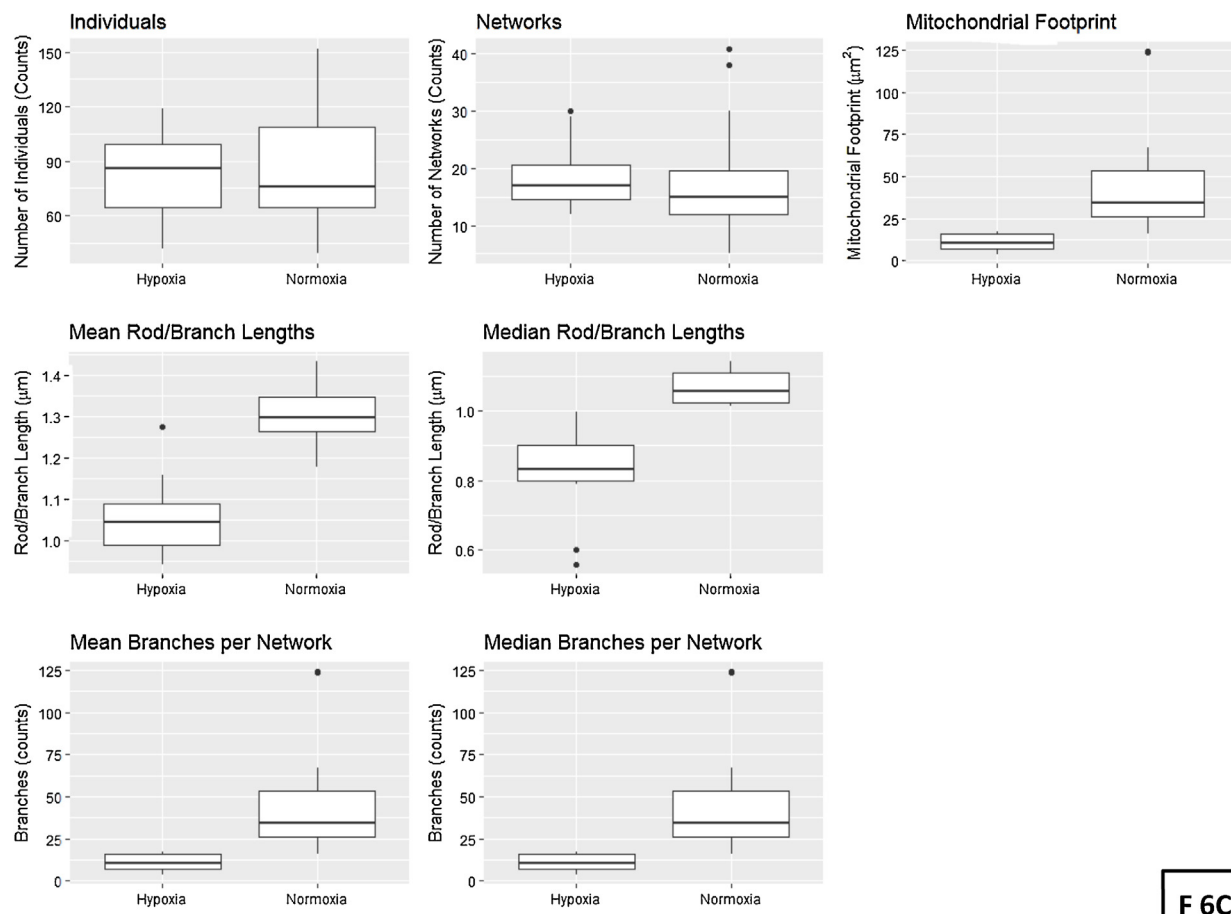
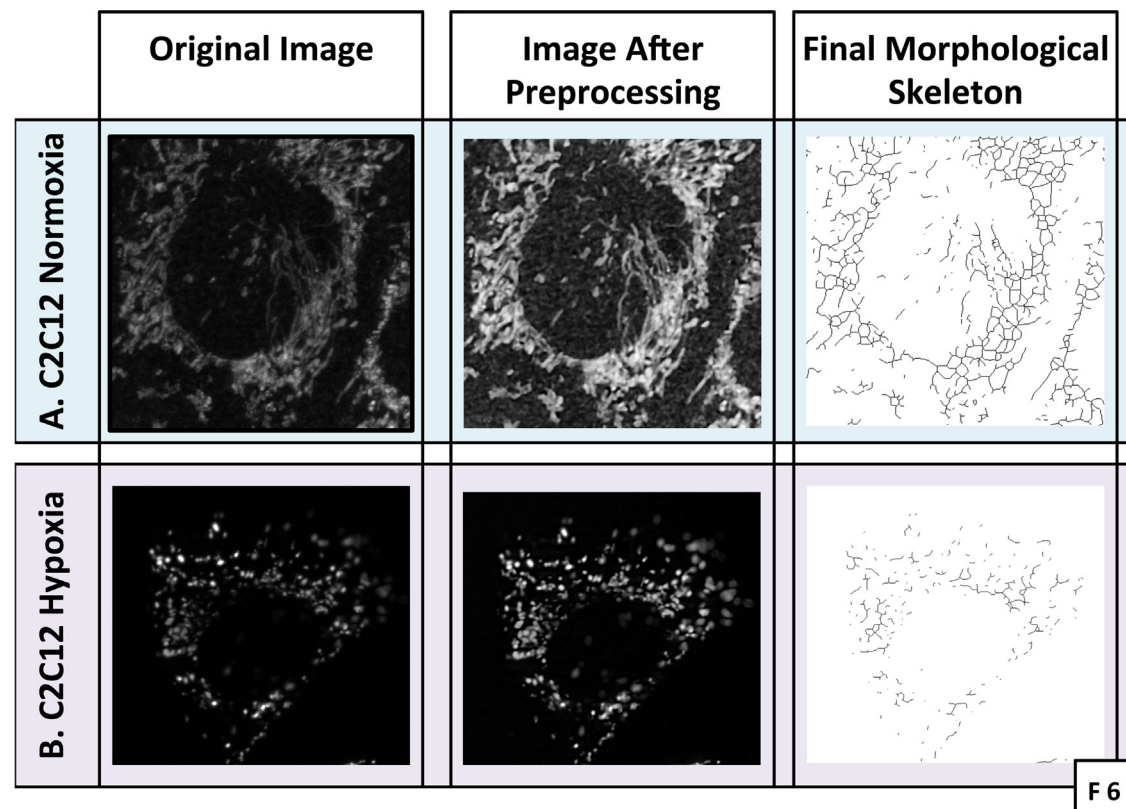


Fig. 6. Results from mitochondrial network analysis performed on fourteen C2C12 cells. (A) A single control cell untreated. (B) A single cell exposed to $<0.1\% \text{ O}_2$ for 24 h. (C) Summary statistics for all cells. Box plots show median (horizontal lines), first to third quartile (box), and the most extreme values within 1.5 times the interquartile range (vertical lines). Differences between control and FCCP treated cells were statistically significant ($p < 0.05$) for all comparisons except Individuals and Networks, using Kruskal Wallis test in R.

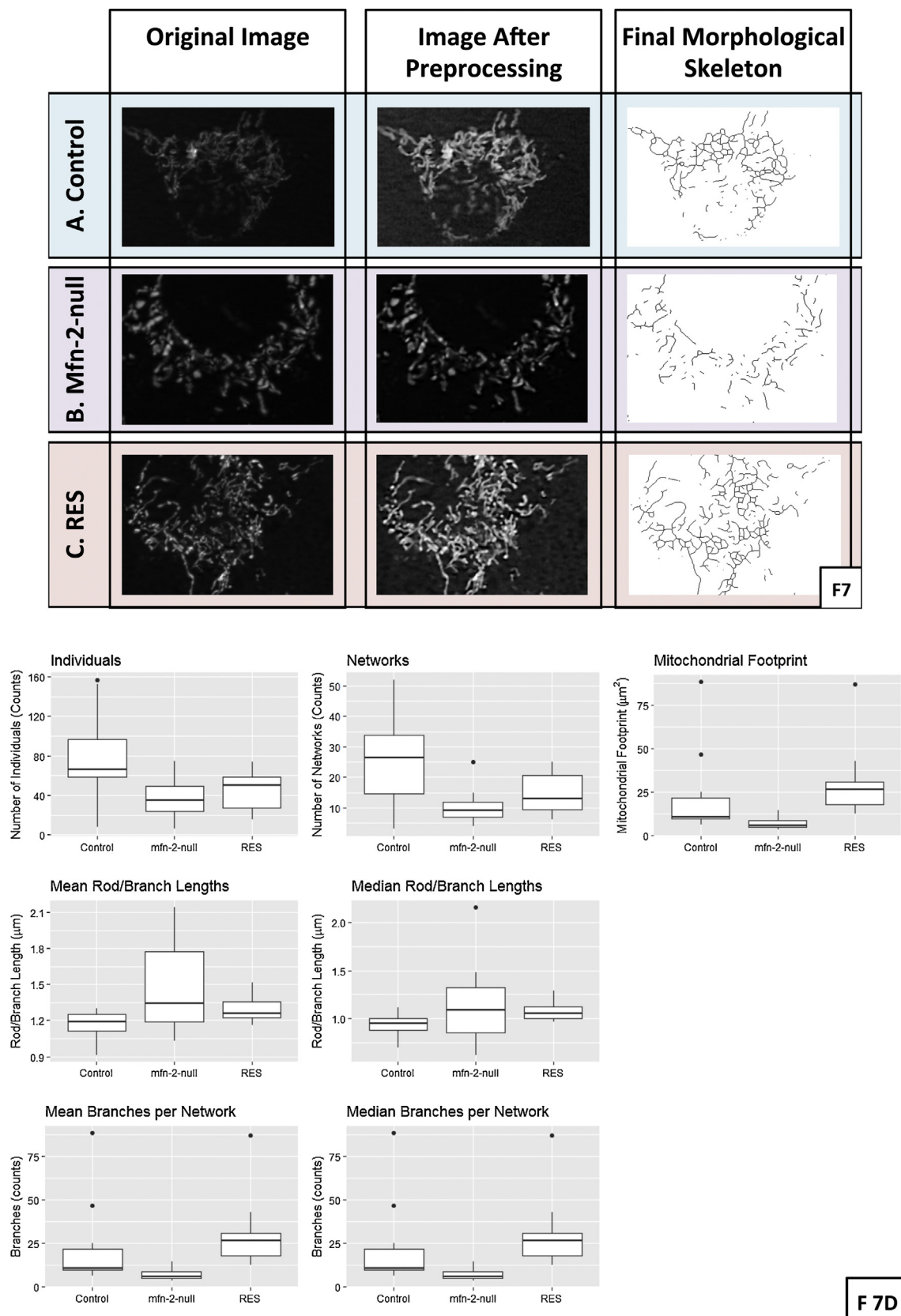


Fig. 7. Results from mitochondrial network analysis performed on 75–110 MEFs. (A) A single wtMEF untreated. (B) A single Mfn2-null MEF untreated. (C) A single wtMEF treated for 48 h with 10 μ M resveratrol (RES). (D) Summary statistics for all cells. Box plots show median (horizontal lines), first to third quartile (box), and the most extreme values within 1.5 times the interquartile range (vertical lines). Differences between control and RES treated cells were statistically significant ($p < 0.05$) for all comparisons, using Kruskal Wallis test in R. Using the kruskalmc functionality of the pgirmess library, the significance between treatments was independently validated. The number of individuals, number of networks, median branches per network, and median rod/branch length were not significantly different ($p > 0.5$) between control and RES groups. The mean length of rods/branches was not significantly different ($p > 0.5$) between the control and Mfn-2-null groups. All other comparisons were found to be statistically significant ($p < 0.5$).

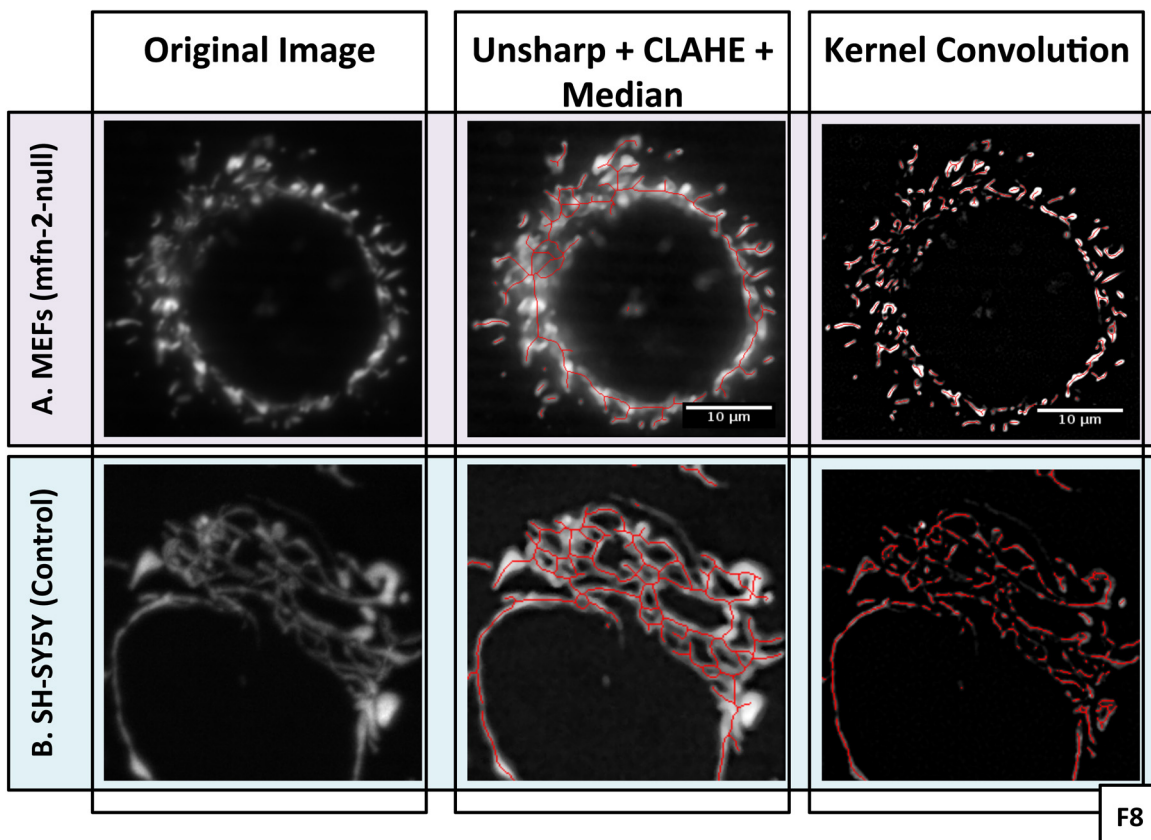


Fig. 8. Comparison of preprocessing using unsharp masking, CLAHE, and median filtering to kernel convolution with a top-hat filter. (A) For the blurry image of the fragmented MEF mfn-2-null mitochondrial material, the kernel convolution provides a more accurate skeleton and thus a better analysis. In contrast, the more connected SH-SY5Y cells (B) are better represented by the skeleton produced from the unsharp mask, CLAHE, and median filtering method.

In general, mitochondrial network morphology is variable between cell types and, whereas in SH-SY5Y cells the networks tend to be simpler, in C2C12 mouse myoblasts they are typically larger and more extensively branched. We have previously observed the extensive fragmentation in C2C12 cells upon exposure to anoxic/hypoxic conditions (unpublished observations, also see Liu and Hajnóczky, 2011). We therefore used this condition to evaluate the ability of MiNA to distinguish between fused and fragmented states. Mitochondrial network skeletons in C2C12 cells labelled with MitoTracker Red were estimated using the sequential application of unsharp mask, CLAHE, and median filtering (Fig. 6A) and then repeated in cells that had been exposed to 0.1% O₂ for 24 h (Fig. 6B; note that this was not lethal). In general, the median numbers of both individuals and networks were substantially greater in C2C12 cells than in SH-SY5Y cells (Fig. 6C), which is consistent with anecdotal observations that the network in C2C12 cells tends to contain many relatively thin interconnected tubular structures. Exposure of C2C12 cells to hypoxia significantly reduced the number of branches per mitochondrial network as well as the mean and median rod/branch length. However, there were no significant effects on the numbers of individuals or networks. This indicates that longer rods are breaking up into smaller rods or punctate and a few larger networks are breaking up into many smaller networks. The mitochondrial footprint was also reduced, again presumably relating to mitophagy under these conditions (Zhang et al., 2008).

MitoTracker Red labelled MEFs were used to investigate the ability of MiNA to identify states of mitochondrial network hyperfusion and fragmentation in a single cell line. We have previously shown the ability of the plant polyphenol resveratrol to stimulate

hyperfusion (Robb et al., 2017; Robb, 2013). In contrast MEFs lacking Mfn2 are highly fragmented (Chen et al., 2005). Therefore, we investigated untreated wtMEFs (Fig. 7A), untreated Mfn2-null MEFs (Fig. 7B), and resveratrol treated wtMEFs (Fig. 7C). Under our conditions, MEFs have mitochondrial network features similar to those of C2C12 cells, with extensive, relatively highly branched networks. MiNA was able to identify reductions in the number of individuals and networks in Mfn2-null MEFs, coincident with reduced mitochondrial footprints, number of branches and rod/branch length. In contrast, resveratrol treatment enhanced all of these features.

Though the workflow used above provided good results in each of these three cases, there is still room for optimization on a case by case basis. Preprocessing methods outside of those proposed here can provide more accurate results under certain conditions. An example, which has been included in the macros as an option, is top hat filtering using a kernel convolution. The seven pixel by seven pixel tophat kernel is described in detail by Iannetti et al. (2016) where Koopman's workflow is extended for high content analysis. The kernel convolution sharpens thin features while reducing high frequency noise. In tests of the kernel's efficacy, we found it could produce more accurate skeleton models from highly fragmented mitochondrial networks in blurry images, such as the mfn-2-null MEFs, compared with the unsharp mask, CLAHE, and median filtering combined (Fig. 8A). However, the skeletons produced in larger and more connected mitochondrial networks, such as those in SH-SY5Y cells, were less accurate when preprocessed using the kernel convolution. These inaccurate skeletons led to the extent of fragmentation being excessively overestimated as regions that appeared to be connected were broken apart by the kernel (Fig. 8B).

Changing the kernel size used by Iannetti et al. (2016) may improve its performance in these instances, and we are currently working on a way to incorporate that option into MiNA in a user-friendly manner.

4. Conclusions

MiNA successfully identified and characterized morphological features of mitochondrial networks in multiple cell lines, and cells in which mitochondria were labelled by either mito-mEFP or Mito-Tracker Red. Fragmentation of the networks and reductions in mitochondrial abundance in response to FCCP uncoupling, hypoxia, and the absence of Mfn-2 was detected. In addition, MiNA could detect differences in network fusion resulting from resveratrol treatment.

It is important to note that, as mitochondrial network morphology becomes increasingly complicated it becomes more probable that erroneous skeletons will be produced. To counter this, the MiNA macros have quality control checkpoints built in where the user is asked to verify that the skeleton produced is an accurate representation, or if the analysis should be aborted so preprocessing procedures may be modified. While this does not solve the issue of erroneous skeletons, it ensures that they are recognized before analysis. In instances where the optional pre-processing does not provide an acceptable skeleton, alternative pre-processing methods may be introduced and used easily since the code is open. Errors may also arise from cells with morphological complexity in three dimensions – more common in thicker cells. The macros currently can only be employed on two dimensional images, though three-dimensional skeletonization has been demonstrated as a useful tool for examining mitochondrial morphology in thicker cells (Nikolaisen et al., 2014) and may be incorporated into the macros in the future.

Acknowledgement

This work was supported by a Natural Science and Engineering Research Council (NSERC) Discovery Grant to JAS (RGPIN-2015-05645).

References

- Ahmad, T., Aggarwal, K., Pattnaik, B., Mukherjee, S., Sethi, T., Tiwari, B.K., Kumar, M., Micheal, A., Mabalirajan, U., Ghosh, B., Sinha Roy, S., Agrawal, A., 2013. Computational classification of mitochondrial shapes reflects stress and redox state. *Cell Death Dis.* 4, e461, <http://dx.doi.org/10.1038/cddis.2012.213>.
- Arganda-Carreras, I., 2016. AnalyzeSkeleton [WWW Document]. ImageJ <http://imagej.net/AnalyzeSkeleton>.
- Arganda-Carreras, I., Fernández-González, R., Muñoz-Barrutia, A., Ortiz-De-Solorzano, C., 2010. 3D reconstruction of histological sections: application to mammary gland tissue. *Microsc. Res. Tech.* 73, 1019–1029, <http://dx.doi.org/10.1002/jemt.20829>.
- Babbar, M., Sheikh, M.S., 2013. Metabolic stress and disorders related to alterations in mitochondrial fission or fusion. *Mol. Cell. Pharmacol.* 5, 109–133, <http://dx.doi.org/10.4255/mcpharmacol.13.11>.
- Benard, G., Bellance, N., James, D., Parrone, P., Fernandez, H., Letellier, T., Rossignol, R., 2007. Mitochondrial bioenergetics and structural network organization. *J. Cell Sci.* 120, 838–848, <http://dx.doi.org/10.1242/jcs.03381>.
- Cereghetti, G.M., Costa, V., Scorrano, L., 2010. Inhibition of Drp1-dependent mitochondrial fragmentation and apoptosis by a polypeptide antagonist of calcineurin. *Cell Death Differ.* 17, 1785–1794, <http://dx.doi.org/10.1038/cdd.2010.61>.
- Chen, H., Chomyn, A., Chan, D.C., 2005. Disruption of fusion results in mitochondrial heterogeneity and dysfunction. *J. Biol. Chem.* 280, 26185–26192, <http://dx.doi.org/10.1074/jbc.M503062200>.
- Chen, H., Vermulst, M., Wang, Y.E., Chomyn, A., Prolla, T.A., McCaffery, J.M., Chan, D.C., 2010. Mitochondrial fusion is required for mtDNA stability in skeletal muscle and tolerance of mtDNA mutations. *Cell* 141, 280–289, <http://dx.doi.org/10.1016/j.cell.2010.02.026>.
- Class UnsharpMask, n.d. Class UnsharpMask [WWW Document]. ImageJ Dev. API Doc. <https://imagej.nih.gov/ij/developer/api/ij/plugin/filter/UnsharpMask.html>.
- Dagda, R.K., 2010. Mitochondrial Morphology [WWW Document]. ImageJ Wiki http://imagejdocu.tudor.lu/doku.php?id=plugin:morphology:mitochondrial_morphology_macro_plugin:start.
- Ferreira, T., Rasband, W., 2012. ImageJ User Guide.
- Galloway, C.A., Lee, H., Yoon, Y., 2012. Mitochondrial morphology – emerging role in bioenergetics. *Free Radic. Biol. Med.* 53, 1–11, <http://dx.doi.org/10.1016/j.freeradbiomed.2012.09.035>.
- Giraudoux, P., 2016. pgirmess: Data Analysis in Ecology.
- Guo, Z., Hall, R.W., 1989. Parallel thinning with two-subiteration algorithms. *Commun. ACM* 32, 359–373, <http://dx.doi.org/10.1145/62065.62074>.
- Iannetti, E.F., Smeitink, J.A.M., Beyrath, J., Willems, P.H.G.M., Koopman, W.J.H., 2016. Multiplexed high-content analysis of mitochondrial morphofunction using live-cell microscopy. *Nat. Protoc.* 11, 1693–1710.
- Ishihara, N., Fujita, Y., Oka, T., Miura, K., 2006. Regulation of mitochondrial morphology through proteolytic cleavage of OPA1. *EMBO J.* 25, 2966–2977, <http://dx.doi.org/10.1038/sj.emboj.7601184>.
- Koopman, W.J.H., Visch, H.J., Smeitink, J.A.M., Willems, P.H.G.M., 2006. Simultaneous quantitative measurement and automated analysis of mitochondrial morphology, mass, potential, and motility in living human skin fibroblasts. *Cytometry A* 69, 1–12, <http://dx.doi.org/10.1002/cyto.a.20198>.
- Landini, G., 2016. Auto Threshold [WWW Document]. ImageJ http://imagej.net/Auto_Threshold.
- Lee, I.H., Finkel, T., 2013. Metabolic regulation of the cell cycle. *Curr. Opin. Cell Biol.* 25, 724–729, <http://dx.doi.org/10.1016/j.ceb.2013.07.002>.
- Lugros, F., Lombès, A., Frachon, P., Rojo, M., 2002. Mitochondrial fusion in human cells is efficient, requires the inner membrane potential, and is mediated by mitofusins. *Mol. Biol. Cell* 13, 4343–4354, <http://dx.doi.org/10.1091/mbc.E02>.
- Leonard, A.P., Cameron, R.B., Speiser, J.L., Wolf, B.J., Peterson, Y.K., Schnellmann, R.G., Beeson, C.C., Rohrer, B., 2015. Quantitative analysis of mitochondrial morphology and membrane potential in living cells using high-content imaging, machine learning, and morphological binning. *Biochim. Biophys. Acta Mol. Cell Res.* 1853, 348–360, <http://dx.doi.org/10.1016/j.bbamcr.2014.11.002>.
- Lihavainen, E., Mäkelä, J., Spelbrink, J.N., Ribeiro, A.S., 2012. Mytoe: automatic analysis of mitochondrial dynamics. *Bioinformatics* 28, 1050–1051, <http://dx.doi.org/10.1093/bioinformatics/bts073>.
- Liu, X., Hajnóczky, G., 2011. Altered fusion dynamics underlie unique morphological changes in mitochondria during hypoxia-reoxygenation stress. *Cell Death Differ.* 18, 1561–1572, <http://dx.doi.org/10.1038/cdd.2011.13>.
- Maddalena, L.A., Ghelfi, M., Atkinson, J., Stuart, J.A., 2017. The mitochondria-targeted imidazole substituted oleic acid “TPP-IOA” affects mitochondrial bioenergetics and its protective efficacy in cells is influenced by cellular dependence on aerobic metabolism. *Biochim. Biophys. Acta Bioenerg.* 1858, 73–85, <http://dx.doi.org/10.1016/j.bbabiobi.2016.11.005>.
- Mitra, K., Wunder, C., Roysam, B., Lin, G., Lippincott-Schwartz, J., 2009. A hyperperfused mitochondrial state achieved at G1-S regulates cyclin E buildup and entry into S phase. *Proc. Natl. Acad. Sci. U. S. A.* 106, 11960–11965, <http://dx.doi.org/10.1073/pnas.0904875106>.
- Nikolaisen, J., Nilsson, L.I.H., Pettersen, I.K.N., Willems, P.H.G.M., Lorens, J.B., Koopman, W.J.H., Tronstad, K.J., 2014. Automated quantification and integrative analysis of 2D and 3D mitochondrial shape and network properties. *PLoS ONE* 9, 1–16, <http://dx.doi.org/10.1371/journal.pone.0101365>.
- Planchon, T.A., Gao, L., Milkiewicz, D.E., Davidson, M.W., Galbraith, J.A., Galbraith, C.G., Betzig, E., 2011. Rapid three-dimensional isotropic imaging of living cells using Bessel beam plane illumination. *Nat. Methods* 8, 417–423, <http://dx.doi.org/10.1038/nmeth.1586>.
- R Core Team, 2016. R: A Language and Environment for Statistical Computing.
- Ridler, T.W., Calvard, S., 1978. Picture thresholding using an iterative selection method. *IEEE Trans. Syst. Man Cybern.* 8, 630–632, <http://dx.doi.org/10.1109/TSMC.1978.4310039>.
- Robb, E.L., Moradi, F., Maddalena, L.A., Valente, A.J.F., Fonseca, J., Stuart, J.A., 2017. Resveratrol stimulates mitochondrial fusion by a mechanism requiring mitofusin-2. *Biochim. Biophys. Res. Commun.* 485, 249–254, <http://dx.doi.org/10.1016/j.bbrc.2017.02.102>.
- Robb, E.L., 2013. Cellular Mechanisms of Resveratrol's Interaction with Mitochondrial Reactive Oxygen Species Metabolism.
- Rossignol, R., Gilkerson, R., Aggeler, R., Yamagata, K., Remington, S.J., Capaldi, R.A., 2004. Energy substrate modulates mitochondrial structure and oxidative capacity in cancer cells. *Cancer Res.* 64, 985–993, <http://dx.doi.org/10.1158/0008-5472.CAN-03-1101>.
- Saalfeld, S., 2010. Enhance Local Contrast (CLAHE) [WWW Document]. ImageJ [http://imagej.net/Enhance_Local_Contrast_\(CLAHE\)](http://imagej.net/Enhance_Local_Contrast_(CLAHE)).
- Salazar-Roa, M., Malumbres, M., 2016. Fueling the cell division cycle. *Trends Cell Biol.* xx, 1–13, <http://dx.doi.org/10.1016/j.tcb.2016.08.009>.
- Schindelin, J., Arganda-Carreras, I., Frise, E., Kaynig, V., Longair, M., Pietzsch, T., Preibisch, S., Rueden, C., Saalfeld, S., Schmid, B., Tinevez, J.-Y., White, D.J., Hartenstein, V., Eliceiri, K., Tomancak, P., Cardona, A., 2012. Fiji: an open-source platform for biological-image analysis. *Nat. Methods* 9, 676–682.
- Schneider, C.A., Rasband, W.S., Eliceiri, K.W., 2012. NIH Image to ImageJ: 25 years of image analysis. *Nat. Methods* 9, 671–675.
- Tufano, M., Cappuccio, G., Terrone, G., Manganelli, F., Pisciotta, C., Geroldi, A., Capponi, S., Del Giudice, E., 2015. Early onset Charcot-Marie-Tooth neuropathy type 2A and severe developmental delay: expanding the clinical phenotype of MNF2-related neuropathy. *J. Peripher. Nerv. Syst.* 20, 415–418, <http://dx.doi.org/10.1111/jns.12148>.
- Twig, G., Elorza, A., Molina, A.J.A., Mohamed, H., Wikstrom, J.D., Walzer, G., Stiles, L., Haigh, S.E., Katz, S., Las, G., Alroy, J., Wu, M., Py, B.F., Yuan, J., Deeney, J.T.,

- Corkey, B.E., Shirihi, O.S., 2008. Fission and selective fusion govern mitochondrial segregation and elimination by autophagy. *EMBO J.* 27, 433–446, <http://dx.doi.org/10.1038/sj.emboj.7601963>.
- Vowinckel, J., Hartl, J., Butler, R., Ralser, M., 2015. MitoLoc: a method for the simultaneous quantification of mitochondrial network morphology and membrane potential in single cells. *Mitochondrion* 24, 77–86, <http://dx.doi.org/10.1016/j.mito.2015.07.001>.
- Wickham, H., 2009. *ggplot2: Elegant Graphics for Data Analysis*. Springer-Verlag, New York.
- Zhang, H., Bosch-Marce, M., Shimoda, L.A., Yee, S.T., Jin, H.B., Wesley, J.B., Gonzalez, F.J., Semenza, G.L., 2008. Mitochondrial autophagy is an HIF-1-dependent adaptive metabolic response to hypoxia. *J. Biol. Chem.* 283, 10892–10903, <http://dx.doi.org/10.1074/jbc.M800102200>.